

Cite this: *Lab Chip*, 2012, **12**, 1262

www.rsc.org/loc

PAPER

Response time of nanofluidic electrochemical sensors†

Shuo Kang, Klaus Mathwig and Serge G. Lemay*

Received 14th November 2011, Accepted 2nd February 2012

DOI: 10.1039/c2lc21104a

Nanofluidic thin-layer cells count among the most sensitive electrochemical sensors built to date. Here we study both experimentally and theoretically the factors that limit the response time of these sensors. We find that the key limiting factor is reversible adsorption of the analyte molecules to the surfaces of the nanofluidic system, a direct consequence of its high surface-to-volume ratio. Our results suggest several means of improving the response time of the sensor, including optimizing the device geometry and tuning the electrode biasing scheme so as to minimize adsorption.

Introduction

Electrochemical (bio)sensors with increasingly complex geometries are being created for integration into lab-on-a-chip systems.^{1–4} One particularly promising approach is so-called redox cycling, in which analyte molecules are repeatedly oxidized and reduced at multiple, closely spaced electrodes. The amplification of faradaic currents inherent to redox cycling can yield important gains in sensitivity and selectivity, while at the same time reducing the volume of sample needed for analysis.^{5–7} A key performance criterion for electrochemical (bio)sensors is speed: for example, the response time of modern commercialized blood glucose meters is typically below 15 seconds.⁸ The factors limiting the response time of “classic” thin-layer cells and the transient response of redox cycling devices have been studied.^{9–11} Additional factors that may be relevant in nanoscale redox cycling devices have however not been explored in detail to date.

Here we present measurements as well as a theoretical analysis of the chronoamperometric transient response of nanoscale redox cycling sensors. Our measurements employ nanogap transducers, which consist of two parallel, closely spaced electrodes separated by a thin (70 nm) liquid-filled channel. By virtue of their geometry, these devices exhibit some of the highest levels of redox cycling amplification reported to date.¹² Surprisingly, we find that the response time of this type of sensor is predominantly limited by adsorption of the redox species onto the channel and electrode surfaces. This increased role for adsorption is a direct consequence of the high surface-to-volume ratio inherent to nanofluidic devices. These results suggest several methods for improving the response time of the devices. Our conclusions are also applicable to other miniaturized electrochemical sensor configurations, especially those based on redox cycling.

Experimental

Nanofluidic devices

Nanogap sensors were fabricated as described previously,¹² except that optical lithography was used to define all the structures instead of electron-beam lithography. In brief, on a 4-inch Si wafer isolated with 500 nm thick thermally grown SiO₂, a 20 nm thick Pt bottom electrode, a 60 nm thick Cr sacrificial layer and a 100 nm thick Pt top electrode were sequentially deposited by electron-beam evaporation and patterned using a lift-off process based on a positive photoresist (OIR 907-17, Arch Chemicals). Afterwards, a passivation layer consisting of 90 nm/325 nm/90 nm thick PECVD SiO₂/SiN/SiO₂ was deposited. Access holes were then etched through the passivation layer in a RIE etcher, reaching the Cr sacrificial layer. Finally, the sacrificial layer was etched by immersing the device in Cr etchant, creating a nanochannel. Fig. 1a shows schematic cross-sections of the devices.

Three designs with different geometries were employed, as shown in Fig. 1b–d. In short, devices of type L10H2 had a 10 μm long detection region with access holes for samples located at both ends of the detection region. Devices of type L50H2 were essentially identical to type L10H2, except that they had a longer (50 μm) active region. Finally, devices of type L50H1 were identical to type L50H2 except that they had only a single access hole located at one end of the active region; the other end of the active region was blocked. Detailed dimensions for the three designs are given in Table 1.

Electrical measurements

Multi-potential-step chronoamperometry measurements were performed with two Keithley 6430 sub-femtoamp remote sourcemeters (Keithley Instruments) that were controlled with in-house LabVIEW software. A standard Ag/AgCl electrode (3 M NaCl, BASi) served both as reference and counter electrode. This configuration is appropriate since the current flowing through the reference electrode is negligibly small.¹² The

MESA+ Institute for Nanotechnology, University of Twente, PO Box 217, 7500 AE Enschede, The Netherlands. E-mail: S.G.Lemay@utwente.nl; Fax: +31 53 489 3511; Tel: +31 53 489 2306

† Electronic supplementary information (ESI) available. See DOI: 10.1039/c2lc21104a

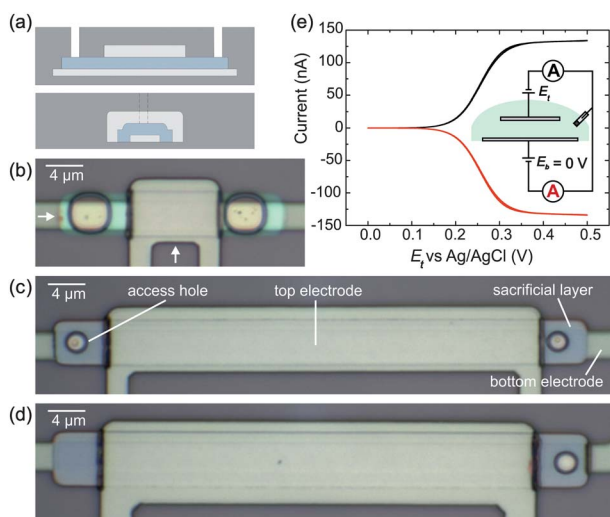


Fig. 1 (a) Schematic device cross-sections along the longitudinal axis (top) and transverse axis (bottom) at the stage prior to Cr etching (not drawn to scale). (b) Optical microscope top view image of the device of type L10H2, in which the sacrificial Cr layer has been etched; the arrows indicate the lines corresponding to the schematic cross-sections in (a). (c) and (d) Devices of type L50H2 and L50H1, respectively, prior to Cr etching. (e) Cyclic voltammetry of a device of type L50H2 filled with 1 mM Fc(MeOH)₂ and 1 M KCl with the potential of the top electrode, E_t , being swept while the potential of the bottom electrode, E_b , was held at 0 V.

Table 1 Dimensions of the three types of devices used in this study

Device name	L10H2	L50H2	L50H1
Length of top electrode/ μm	10	50	50
Width of top electrode/ μm	5	5	6
Width of bottom electrode/ μm	3	3	3
Number of access holes	2	2	1
Size of access hole(s) ^a / $\mu\text{m} \times \mu\text{m}$	4×4	2×2	2×2
Distance of the access hole(s) from the edge of the top electrode ^b / μm	2	2	2

^a The corners of the access holes become rounded during lithography.

^b There is some random offset in the real devices compared to the mask design due to the alignment tolerance in lithography.

reference electrode was immersed in a PDMS reservoir with an opening at the bottom that contacted the device.

Chemicals

Ferrocenedimethanol, Fc(MeOH)₂, was purchased from Acros (cat. no. 382550010), and potassium chloride, KCl, from Sigma-Aldrich (cat. no. P3911). The chromium etchant (Selectipur) was from BASF and the sulfuric acid, H₂SO₄, from Sigma-Aldrich (cat. no. 339741). All chemicals were used as received and the solutions were prepared using 18.2 M Ω cm MilliQ water.

Electrode cleaning

Prior to electrochemical measurements, the devices were cleaned by filling with a solution of 0.5 M H₂SO₄ and repeatedly

sweeping the electrode between -0.15 V and 1.15 V vs. Ag/AgCl until a reproducible voltammogram was obtained.

Results and discussions

The basic operation of a device of type L50H2 is illustrated in Fig. 1e, which shows a cyclic voltammogram in the presence of 1 mM Fc(MeOH)₂ and 1 M KCl as the supporting electrolyte. The steady-state oxidation current collected at the top electrode is equal and opposite to the reduction current collected at the bottom electrode, as expected for redox cycling. Because the kinetics of Fc(MeOH)₂ are essentially reversible under the present conditions,¹² the magnitude of the steady-state current, i_{ss} , is simply given by diffusive mass transport combined with the Nernst equation,¹³

$$i_{\text{ss}} = \frac{nFADc_b}{z} \left(\frac{1}{1 + e^{-f\eta_t}} \right). \quad (1)$$

Here n is the number of electrons transferred per molecule ($n = 1$ for Fc(MeOH)₂), F the Faraday constant, A the overlap area between top and bottom electrodes, D the diffusion coefficient (5.6×10^{-6} cm² s⁻¹ for Fc(MeOH)₂[‡]), c_b the bulk concentration of the redox species, $f = F/RT$ with R the gas constant and T the absolute temperature, $\eta_t = E_t - E^0$ the overpotential applied to the top electrode, and z the distance between the two electrodes. The latter has a value $z = 70$ nm, as deduced from the diffusion-limited steady-state current at high overpotential ($f\eta_t \gg 1$). This is slightly higher than the thickness of the sacrificial Cr layer (60 nm), which we attribute to slight buckling of the top electrode after the sacrificial Cr layer was etched.

Multi-potential-step chronoamperometry

To investigate the transient response of the devices, we filled a device with an aqueous solution of 1 mM Fc(MeOH)₂ and 1 M KCl as the supporting electrolyte. We then applied a series of step-wise perturbations to the biasing potential of one of the electrodes while holding the potential of the other electrode fixed. The resulting electrochemical current response was measured as a function of time. For example, Fig. 2a shows the potentials applied to the two electrodes of a device of type L50H2; the potential of the bottom electrode was kept at 0 V while the top electrode was stepped at regular intervals. The resulting current-time response is shown in Fig. 2b.

Each time that the voltage applied to the top electrode was stepped, the redox cycling current suddenly jumped to a different value, then gradually settled to a new steady-state current. This new steady-state current corresponded to the value i_{ss} given by eqn (1), as expected. Importantly, however, increasing the voltage typically caused the current to initially jump to a value *lower* than i_{ss} , a counterintuitive behaviour that cannot be predicted from inspection of the steady-state voltammogram. Conversely, stepping the potential downward typically caused an initial *increase* in the current. Furthermore, the duration of the transient was longer for more positive potentials at the top electrode, indicating that the dynamic response of the device is limited by a potential-dependent effect.

[‡] Determined from the diffusion-limited current at a 5 μm radius platinum ultramicroelectrode.

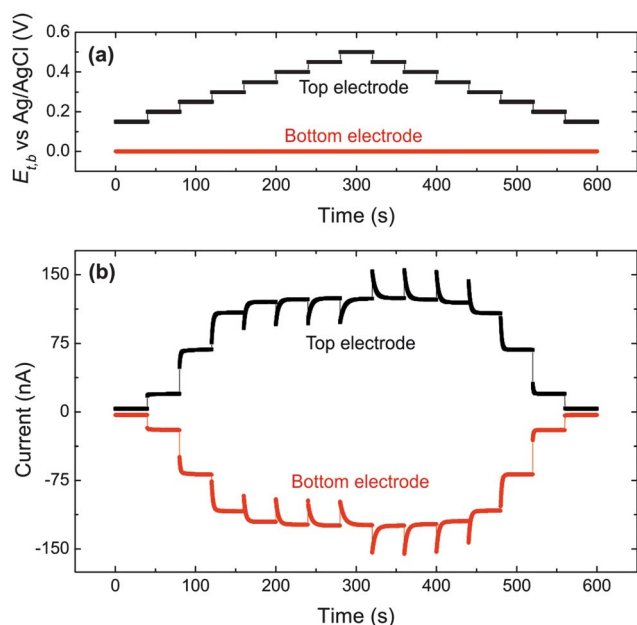


Fig. 2 Multi-potential-step chronoamperometry of a device of type L50H2 filled with an aqueous solution of 1 mM $\text{Fc}(\text{MeOH})_2$ and 1 M KCl as the supporting electrolyte. (a) Potentials applied as a function of time to the top (black) and bottom (red) electrode. (b) Corresponding current–time response.

To better quantify this potential dependence, a modified multi-potential-step chronoamperometry measurement was carried out in which the potential of the bottom electrode was kept at 0 V while a sequence of potential steps was applied to the top electrode, as shown in Fig. 3a. Before each step, the potential of the top electrode was returned to 0 V so as to initialize the device to the same state. The corresponding amperometric response is illustrated in Fig. 3b (a similar experiment in which the bottom electrode was kept at 0.5 V, an oxidizing potential, instead of 0 V, a reducing potential, is shown in the ESI†). No current flowed in the “initialization” stages where both top and bottom electrodes were biased at 0 V, as expected. When the potential of the top electrode was stepped up, the current first jumped to a finite value, then continued to increase gradually until the steady-state current i_{ss} was approached. Higher potentials resulted in longer transients and larger departures of the current from its steady-state value in the early part of the transients.

Quantitatively, the response time t_{90} (defined as the time to reach 90% of i_{ss} after a perturbation) increased from 5.3 s to 8.1 s and 11.1 s when stepping from 0 V to 0.4 V, 0.45 V and 0.5 V, respectively. For a linear system, one would expect the response time to be independent of the size of the stimulus step. The experimental results therefore indicate that, surprisingly, the response is not linear in the applied voltage.

To quantify the magnitude of the transient, we define the transient fraction, F_{TS} , as the ratio of the current excursion away from its new steady-state value, Δi , and the current level at steady state i_{ss} : $F_{TS} = \Delta i/i_{ss}$. For steps to 0.4 V, 0.45 V and 0.5 V in Fig. 3, the observed transient fractions were 75%, 84% and 89%, respectively. Once again, the dependence of the transient fraction on the size of the potential step reflects an underlying nonlinearity.

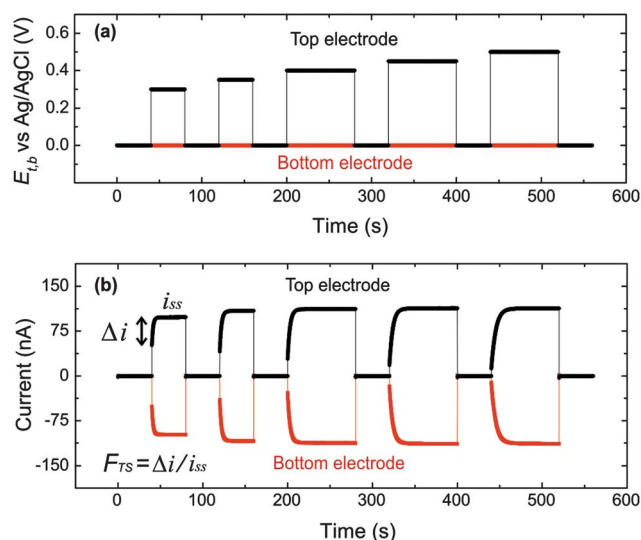


Fig. 3 Modified multi-potential-step chronoamperometry of a device of type L50H2 filled with an aqueous solution of 1 mM $\text{Fc}(\text{MeOH})_2$ and 1 M KCl as the supporting electrolyte. (a) Potentials applied as a function of time to the top (black) and bottom (red) electrode. (b) Corresponding current–time response.

Transient response analysis

The above results show that the response time of the device varies from a few to a dozen seconds depending on the biasing potential. Several possible mechanisms can be ruled out as the origin because they take place in much shorter time scales: the source-meters have a rise time of several ms, much faster than the observed response; we estimate the RC time of capacitive currents due to charging of the ionic double layer at the electrodes to be only 0.53 ms, as discussed further in the ESI†; and the concentration gradient of redox molecules across the nanochannel is established on a time scale $\tau = z^2/2D = 4.4 \mu\text{s}$ after a change in potential, again much shorter than the observed response.

As argued in detail below, we instead interpret the long transient time as the slow diffusive response to *potential-dependent adsorption*.¹⁴ A change in adsorption of redox molecules at the electrodes after a voltage step causes a temporary concentration difference between the nanochannel and external reservoir; to bring the concentration back into equilibrium, molecules need to diffuse along the length of the nanochannel.

In a first estimate, the time for molecules to diffuse from the access holes of a nanochannel to its centre can be approximated by $(L/2)^2/2D$, where L is the length of the channel. For device type L50H2, this gives a value of 0.65 s. While shorter than the transient times observed in Fig. 2 and 3, this already suggests that longitudinal diffusion of the redox-active species along the length of the device may indeed be implicated in the observed slow response.

To further test this interpretation, we measured the response time of the three device geometries listed in Table 1 under identical measurement conditions. The expected ratio of response time between devices of type L10H2, L50H2 and L50H1 was 1 : 15 : 55 ($L/2 = 7 \mu\text{m}$ and $27 \mu\text{m}$ for devices of type L10H2 and L50H2, respectively; for type L50H1, $L = 52 \mu\text{m}$

should be used instead of $L/2$ for the estimation due to the unique access hole at the end of the channel). The measured current responses, $i(t)/i_{ss}$, are shown in Fig. 4a. The observed response times were $t_{90} = 0.31$ s, 5.5 s and 19.5 s, corresponding to a ratio 1 : 18 : 65 and consistent with the above estimate. This supports the hypothesis that longitudinal diffusion is responsible for the observed transient response.

In addition to correctly predicting the dependence of t_{90} on geometry, longitudinal diffusion can also quantitatively explain the counterintuitive transient shape observed in Fig. 2 and 3. At any given moment, the redox-cycling current $i(t)$ is proportional to $\bar{c}(t)$, the concentration of redox species present in the channel averaged over the volume of the channel:

$$i(t) = \frac{\bar{c}(t)}{c_b} i_{ss} \quad (2)$$

When a potential step is applied, the distribution of molecules inside the channel is altered, resulting in a transient $\bar{c}(t)$. To determine the theoretically expected form of $\bar{c}(t)$, we numerically solved the diffusion equation, $\partial c/\partial t = D_{\text{eff}} \partial^2 c/\partial x^2$, as detailed in the ESI†. Here D_{eff} is an effective diffusion coefficient inside the channel, as discussed further below. The numerical solutions for the current are well described by an analytical expression,

$$i(t) = i(0^+) + (i_{ss} - i(0^+)) \text{erf} \left(2.97\gamma \left(\frac{D_{\text{eff}} t}{L^2} \right)^{0.6} \right), \quad (3)$$

where $i(0^+)$ is the value of current immediately after the potential step, i_{ss} is the new steady-state current and γ is a numerical constant with a value $\gamma = 1$ and 0.60 for devices with two and one access hole(s), respectively. This analytical form can be fitted to the experimental data and the value of D_{eff} can be extracted.

Fits of the measured current transients to eqn (3) are shown in Fig. 4a. The shape of the transients matches very well with the fits, which provides strong evidence that the dynamic response of the nanofluidic device is indeed determined by longitudinal diffusion of the analyte molecules in the nanochannel. The fitted values of the effective diffusion constant, $8.0 \times 10^{-7} \text{ cm}^2 \text{ s}^{-1}$, $8.5 \times 10^{-7} \text{ cm}^2 \text{ s}^{-1}$ and $5.4 \times 10^{-7} \text{ cm}^2 \text{ s}^{-1}$ for the device of type L10H2, L50H2 and L50H1, respectively, are however one order of magnitude smaller than the diffusion constant measured in bulk ($5.6 \times 10^{-6} \text{ cm}^2 \text{ s}^{-1}$). This indicates that diffusion of the redox species in the channel is dramatically slowed down compared to that in bulk solution.

Adsorption-limited diffusion

Our experimental data exhibit two unexpected features. First, changing the potential of an electrode leads to temporary decreases or increases in the channel concentration $\bar{c}(t)$. Second, the effective diffusion coefficient in the channel, D_{eff} , is smaller than the bulk diffusion coefficient, resulting in longer transients than expected from unconstrained diffusion. We propose that both of these effects share a common origin, namely, reversible adsorption of the analyte molecules onto the channel walls. Adsorption plays a particularly important role in nanochannels due to their high surface-to-volume ratio, and it is well documented that dynamic adsorption results in an apparent decrease of the diffusion coefficient.^{14–19,21} Furthermore, the degree of adsorption of redox species to an electrode was shown to depend on the potential applied to that electrode.¹⁴ As a consequence, molecules are adsorbed or desorbed when changing the potential at an electrode, resulting in the temporary depletion or accumulation of redox molecules inside the channel.

The adsorption scenario corresponding to the data of Fig. 2 and 3 is illustrated in Fig. 5. In the first case considered, shown in the left column, the potential of the top electrode is stepped from 0 V to 0.5 V while the potential of the bottom electrode is kept at 0 V. At time t_1 , before the potential step, all the molecules are in the reduced form; the concentration of analyte molecules in the nanochannel, $\bar{c}(t_1)$, then equals the bulk concentration in the external reservoir, c_b , and there is no faradaic current. Some molecules are additionally adsorbed to the electrode surfaces. When the potential of the top electrode is stepped to 0.5 V at time t_2 , redox cycling starts and molecules are oxidized at the top electrode. If these oxidized molecules adsorb more strongly to the top electrode than the reduced molecules did prior to the voltage step, the number of diffusing molecules remaining in the channel is temporarily decreased. Consequently, more molecules must

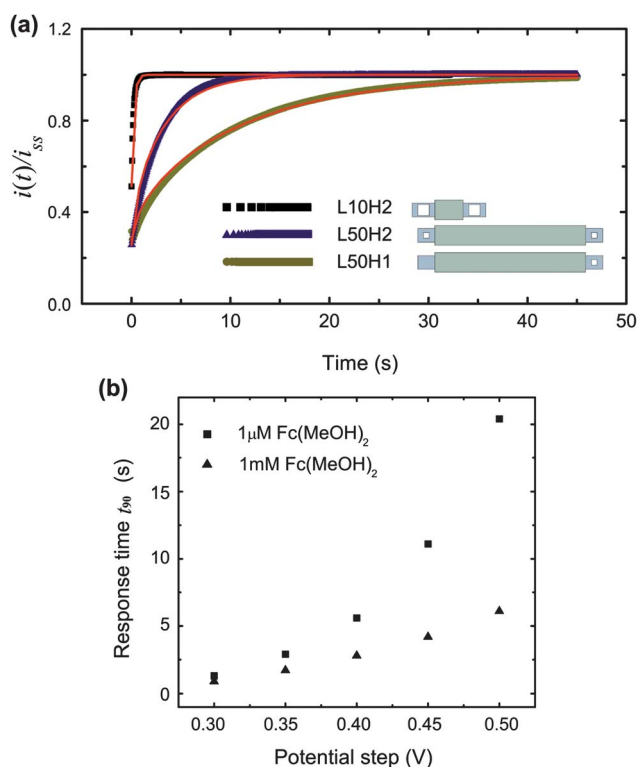


Fig. 4 (a) Measured current responses $i(t)/i_{ss}$ of devices of type L10H2, L50H2 and L50H1 to a potential perturbation from 0 V to 0.4 V applied to one electrode while keeping the other electrode at 0 V. The red lines are fit to eqn (3). (b) Response time t_{90} of the device of type L50H2 to potential steps with different magnitudes in 1 mM Fc(MeOH)₂ (triangle) and 1 μM Fc(MeOH)₂ (square). In order to obtain comparable data, the same device was used for all the measurements and the electrode was cleaned with H₂SO₄ before each measurement.

§ The scenario is based on the assumption that the adsorption and desorption time are much shorter than the typical time for molecules to diffuse through the channel.¹⁹

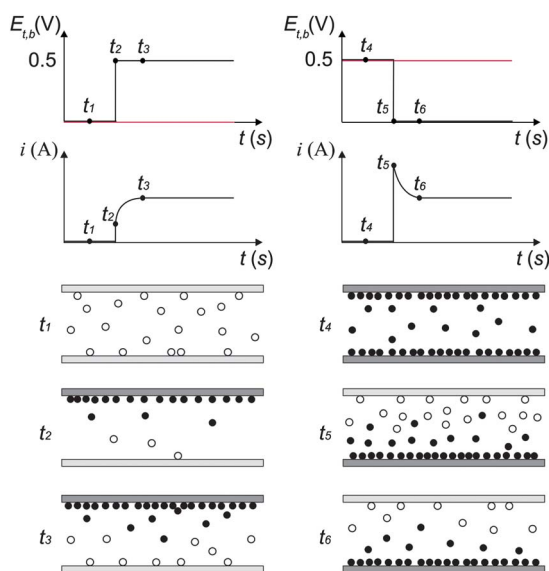


Fig. 5 Adsorption (left column) and desorption (right column) scenario.

enter the channel from the outside reservoir so as to re-establish the concentration balance until, at time t_3 , the bulk concentration in the nanochannel, $\bar{c}(t_3)$, equals the bulk concentration, c_b , and a new steady state is approached. At time t_2 , stepping to a higher potential causes more molecules to be adsorbed, leaving fewer freely diffusing molecules in the channel, and causing the initial current to depart further from the new steady-state value. This shows how, in Fig. 3b, F_{TS} can increase with the biasing potential of the top electrode. Higher adsorption further means that D_{eff} decreases with increasing potential, which in turn causes the transients to last longer at the higher top electrode potential, as observed.

The reverse effect is sketched in the right column of Fig. 5. Before the potential step, at time t_4 , both of the electrodes are biased at 0.5 V, all the molecules inside the nanochannel are oxidized ($\bar{c}(t_4) = c_b$), and no redox cycling current is generated. Additional oxidized molecules are adsorbed to the electrode surfaces. At time t_5 , when the potential of the top electrode drops from 0.5 V to 0 V, redox cycling starts and molecules desorb from the electrode, temporarily increasing the concentration of freely diffusing molecules in the channel, and hence the current then gradually decreases until diffusive equilibrium with the external reservoir is re-established. This effect is responsible for the current increases observed in the second half of Fig. 2b.

The data above are representative of measurements on more than 20 devices. We have however observed that D_{eff} , and therefore the amount of adsorption, varied slowly over time for a given device. For example, storing devices for a day in MilliQ water usually resulted in a smaller value of D_{eff} . Occasionally, devices with a freshly etched Cr sacrificial layer exhibited opposite tendencies to those of Fig. 2 and 3, as shown in the ESI†. Such sample history dependence is not surprising since adsorption is extremely sensitive to trace contaminants on the channel surfaces. Cleaning with H_2SO_4 , as described in the Experimental section, helped to ensure reproducible starting conditions.

Improving the response time of nanogap transducers

The above finding that the transient response of nanofluidic thin-layer cells is dominated by adsorption suggests several ways to improve the response time of the sensor.

For adsorption-limited diffusion, the mean time for molecules to diffuse along the channel scales as the square of the length of the device. A short device provides a faster response, but at the cost of lower signal levels. By designing long devices with multiple access holes, or building multiple short devices in parallel, the response time can be shortened while maintaining high signal levels.

Less intuitively, Fig. 2b and 3b show that the response time is influenced by the biasing potential. This is further demonstrated in Fig. 4b, which shows the response time as a function of electrode potential for two concentrations of $\text{Fc}(\text{MeOH})_2$ in 1 M KCl. The response time at low concentration (1 μM $\text{Fc}(\text{MeOH})_2$) was longer than that at high concentration (1 mM $\text{Fc}(\text{MeOH})_2$). This indicates that adsorption is more pronounced at low concentrations. This observation is consistent with the commonly observed Freundlich adsorption isotherm,²⁰ as well as consistent with previous observations in nanogap devices.²¹ Importantly, the response times also increased with increasing electrode potential. This is a very significant effect: with 1 mM $\text{Fc}(\text{MeOH})_2$, the response time increased from 2.8 s to 6.1 s for electrode potentials of 0.4 V and 0.5 V, respectively, even though both of these potentials are sufficiently high that the diffusion-limited steady-state current is observed in both cases. Similarly, with 1 μM $\text{Fc}(\text{MeOH})_2$, the response time went from 5.6 s to 20.4 s at these potentials. This therefore leads to the important conclusion that the response time of redox cycling sensors can be decreased significantly without loss of signal by choosing operating potentials that minimize adsorption.

Finally, it has been shown that functionalization of the electrodes with self-assembled monolayers of organothiol molecules bearing polar end groups can reduce adsorption.¹⁴ The present analysis indicates that doing so would correspondingly improve the response time of redox cycling sensors.

Conclusions

We have found that the chronoamperometric response time of redox cycling nanofluidic thin-layer cells is limited by adsorption of redox molecules to the nanochannel surface. Observed trends in the duration, the magnitude, the dependence on device geometry and on electrode potential of the transients are consistent with this interpretation, and the experimentally observed form of the transients is in excellent agreement with simulations based on diffusive mass transport. The observed response times were found to be an order of magnitude longer than expected if adsorption is not taken into account. These findings have important consequences for the design of thin-layer cell sensors since the slowing effect of adsorption can be mitigated by an appropriate choice of electrode material, device geometry and bias potential.

Acknowledgements

The authors gratefully acknowledge financial support from the Netherlands Organization for Scientific Research (NWO) and the European Research Council (ERC).

References

- 1 N. J. Ronkainen, H. B. Halsall and W. R. Heineman, *Chem. Soc. Rev.*, 2010, **39**, 1747–1763.
- 2 D. Wei, M. J. A. Bailey, P. Andrew and T. Ryhänen, *Lab Chip*, 2009, **9**, 2123–2131.
- 3 D. Grieshaber, R. MacKenzie, J. Vörös and E. Reimhult, *Sensors*, 2008, **8**, 1400–1458.
- 4 L. Nyholm, *Analyst*, 2005, **130**, 599–605.
- 5 O. Niwa, Y. Xu, H. B. Halsall and W. R. Heineman, *Anal. Chem.*, 1993, **65**(11), 1559–1563.
- 6 E. Kätelhön, B. Hofmann, S. G. Lemay, M. A. G. Zevenbergen, A. Offenhäusser and B. Wolfrum, *Anal. Chem.*, 2010, **82**(20), 8502–8509.
- 7 M. Schienle, C. Paulus, A. Frey, F. Hofmann, B. Holzapfl, P. Schindler-Bauer and R. Thewes, *IEEE J. Solid-State Circuits*, 2004, **39**(12), 2438–2445.
- 8 J. D. Newman and A. P. F. Turner, *Biosens. Bioelectron.*, 2005, **20**, 2435–2453.
- 9 K. Yamada, F. Kitamura, T. Ohsaka and K. Tokuda, *J. Electrochem. Soc.*, 1996, **143**, 4006–4012.
- 10 J. E. Devilbiss, J. X. Wang, B. M. Ocko, K. Tamura, R. R. Adzic, I. A. Vartanyants and I. K. Robisonson, *Electrochim. Acta*, 2002, **47**, 3057–3064.
- 11 R. D. Martin and P. R. Unwin, *Anal. Chem.*, 1998, **70**, 276–284.
- 12 M. A. G. Zevenbergen, B. L. Wolfrum, E. D. Goluch, P. S. Singh and S. G. Lemay, *J. Am. Chem. Soc.*, 2009, **131**, 11471–11477.
- 13 A. J. Bard and L. R. Faulkner, *Electrochemical Methods: Fundamentals and Applications*, Wiley, New York, 2001.
- 14 P. S. Singh, H. M. Chan, S. Kang and S. G. Lemay, *J. Am. Chem. Soc.*, 2011, **133**(45), 18289–18295.
- 15 K. Pappaert, J. Biesemans, D. Clicq, S. Vankrunkelsven and G. Desmet, *Lab Chip*, 2005, **5**, 1104–1110.
- 16 N. F. Y. Durand, A. Bertsch, M. Todorova and P. Renaud, *Appl. Phys. Lett.*, 2007, **91**, 203106.
- 17 N. F. Y. Durand, C. Dellagiacomma, R. Goetschmann, A. Bertsch, I. Märki, T. Lasser and P. Renaud, *Anal. Chem.*, 2009, **81**, 5407–5412.
- 18 I. De Santo, F. Causa and P. A. Netti, *Anal. Chem.*, 2010, **82**, 997–1005.
- 19 A. Grattoni, J. Gill, E. Zabre, D. Fine, F. Hussain and M. Ferrari, *Anal. Chem.*, 2011, **83**, 3096–3103.
- 20 J. Lyklema, *Fundamentals of Interface and Colloid Science Volume 1: Fundamentals*, Academic Press, London, 1991.
- 21 M. A. G. Zevenbergen, P. S. Singh, E. D. Goluch, B. L. Wolfrum and S. G. Lemay, *Anal. Chem.*, 2009, **81**, 8203–8212.

Supporting Information for: Response Time of Nanofluidic Electrochemical Sensors

Shuo Kang, Klaus Mathwig and Serge G. Lemay

MESA+ Institute for Nanotechnology, University of Twente, PO Box 217,
7500 AE Enschede, the Netherlands

A. Multi-potential-step chronoamperometry

Figure S1 shows an experiment complementary to the one of Figure 3: The bottom electrode was kept at 0.5 V instead of 0 V while the potential of the top electrode was stepped. Current transients were observed when the top electrode potential was stepped to the base level of 0 V, which corresponds to diffusion-limited mass transport. The shape of the transient depended on the potential of the top electrode prior to the potential step, the magnitude of the transient fraction is larger for higher starting potentials. Specifically, when the potential of the top electrode was stepped from 0.4 V, 0.45 V and 0.5 V to 0 V, the current increased to 129 nA, 133 nA and 139 nA, respectively.

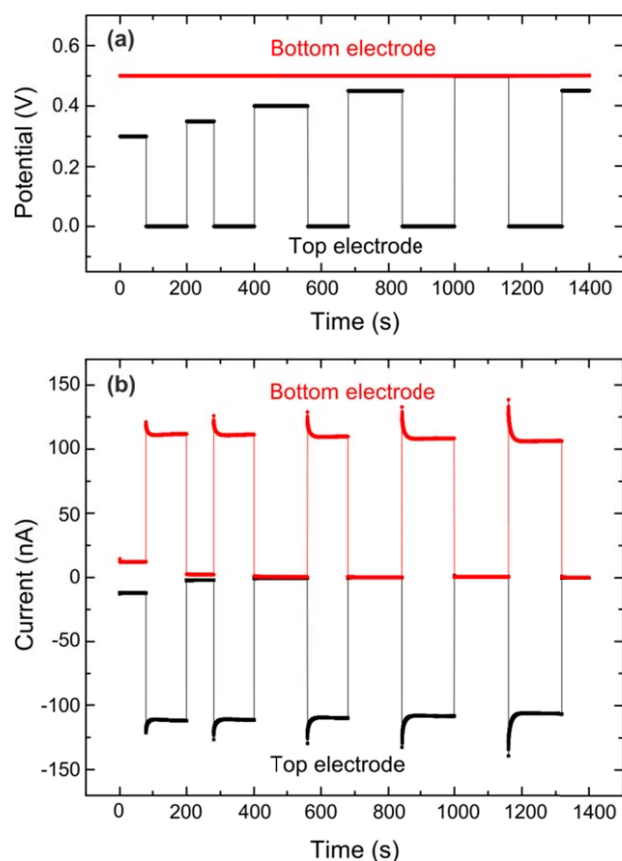


Fig. S1 Multi-potential-step chronoamperometry of a device of type L50H2 filled with an aqueous solution of 1 mM Fc(MOH)₂ and 1 M KCl as supporting electrolyte. (a) Potentials applied as a function of time to the top (black) and bottom (red) electrode. (b) Corresponding current-time responses.

B. RC charging time of the device

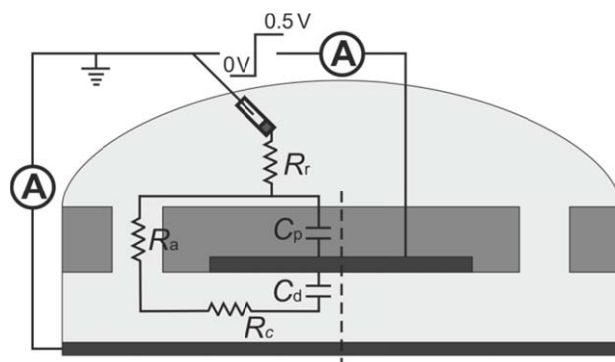


Fig. S2 Equivalent circuit diagram of the nanofluidic system.

Here we estimate the RC charging time when stepping the potential of the top electrode (geometry of the device of type L50H2 is used). The equivalent circuit for this case is shown in Figure S2. The various parameters in Figure S2, as well as estimates for their numerical values, are as follows :

- C_p This represents the capacitance between bulk solution and the electrode across its protective passivation layer. The passivation layer consists of 90 nm/325 nm/90 nm thick SiO₂/SiN/SiO₂. The total capacitance is therefore given by the individual capacitances contributed by these three layers connected in series. Using a relative permittivity of $\epsilon_r = 7$ for PECVD SiN, $\epsilon_r = 5$ for PECVD SiO₂, and an area $A \approx 1000 \mu\text{m}^2$ (including $350 \mu\text{m}^2$ for the top electrode itself and about $650 \mu\text{m}^2$ for its contacting wire exposed to solution) yields a total capacitance $C_p \approx 0.1 \text{ pF}$.
- C_d This represents the ionic double layer capacitance. At a given potential, the double layer capacitance per unit area is typically in the range of 10 to 40 $\mu\text{F}/\text{cm}^2$.[†] Using $A = 175 \mu\text{m}^2$, which is half of the top electrode area (for a symmetric device with two access holes), yields C_d in the range of 18 to 70 pF.
- R_a The resistance of the cylindrical access hole is given by $l/\kappa\pi r^2 = 16 \text{ k}\Omega$, where $l = 505 \text{ nm}$ is the depth of the access hole, $r = 1 \mu\text{m}$ is its radius, and κ is the conductivity of the solution, which is $10.2 \Omega^{-1}\text{m}^{-1}$ for 1 M KCl at 20°C. The spreading resistance in the vicinity of the entrance hole contributes an additional resistance $1/4\kappa r = 25 \text{ k}\Omega$, for a total access resistance $R_a = 41 \text{ k}\Omega$.
- R_r The resistance of the bulk solution, R_r , is dominated by the spreading resistance in the region near the device. A rough estimate is $R_r = 1/4\kappa L = 500 \Omega$, which indicates that it can be neglected.
- R_c The resistance of (half of) the nanochannel, R_c , is equal to $L/\kappa hW = 7.6 \text{ M}\Omega$, where $L = 27 \mu\text{m}$ is half of the length of the nanochannel, $h = 70 \text{ nm}$ and $W = 5 \mu\text{m}$ are the height and width of the nanochannel, respectively.

[†] A. J. Bard, L. R. Faulkner, *Electrochemical Methods: Fundamentals and Applications*, Wiley: New York, 2001.

The above indicates that the capacitance of the passivation layer is utterly negligible compared to the double-layer capacitance, despite the additional area relevant for C_p . Similarly, the resistance in series with the double layer capacitance is dominated by the nanochannel itself by virtue of its small cross-sectional area. An upper bound for the dominant RC time constant is therefore estimated as $\tau = (R_r + R_a + R_c) C_d = 0.53$ ms. This is orders of magnitude shorter than the transients observed in the experiments, indicating that the latter have a different origin. A corresponding calculation for the bottom electrode yields a similarly short RC time constant.

In addition to estimating the RC time constant, we measured the current response of a device of type L50H1 filled with only supporting electrolyte to the potential steps applied as in Figure 3(a). Keeping the potential of bottom electrode at 0 V, without any redox species present in the nanochannel, positive or negative current spikes were observed at the top electrode when its potential was stepped upward or downward, respectively. The transients lasted ~ 0.2 s, significantly shorter than those observed in the experiments with redox molecules. This shows that the slow response in the latter experiments was not caused by charging effects. To understand the difference between the observed response and the numerical estimate of the RC time given above, note that besides RC charging, dielectric relaxation of the passivation material ($\text{SiO}_2/\text{SiN}/\text{SiO}_2$)^{1,2,3} also contributes to (and in fact dominates) the measured current.

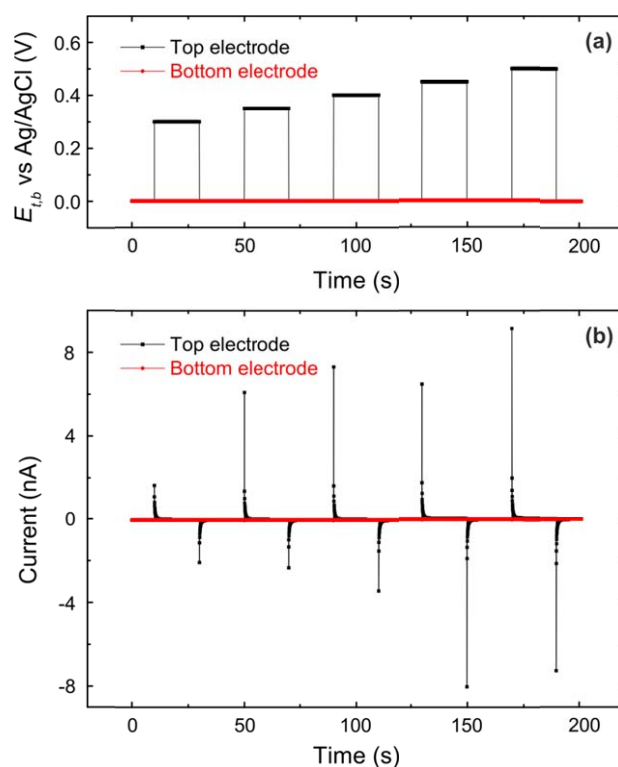


Fig. S3 Transient response of a device of type L50H1 filled with only supporting electrolyte of 1 M KCl. (a) Potentials applied as a function of time to the top (black) and bottom (red) electrode. (b) Corresponding current-time responses.

¹D. Krapf, M. Wu, R. M. M. Smeets, H. W. Zandbergen, C. Dekker, and S. G. Lemay, *Nano Lett.*, 2006, **6**(1), 105-109.

²A. K. Jonscher, *Nature*, 1977, **267**, 673-679.

³S. Westerlund, L. Ekstam, *IEEE Trans. Dielectr. Insul.*, 1994, **1**(5), 826-839.

C. Determination of the transient response

We obtained the expression for the transient response of the current, equation (3), as a purely phenomenological fit to the numerically determined diffusion of molecules into the channel.

The one-dimensional diffusion equation,

$$\frac{\partial c(x, t)}{\partial t} = D \frac{\partial^2 c(x, t)}{\partial x^2},$$

was solved numerically along the length L of a nanochannel using the following initial and boundary conditions:

– Initially, no redox active molecules are present in the channel. Hence, the starting condition for $t = 0$ is

$$c(x, 0) = 0 \text{ for } 0 < x < L.$$

– The bulk concentration at the edge of the nanochannel that is connected to the reservoir is kept constant at c_b for all times t :

$$c(x = 0, t) = c(x = L, t) = c_b.$$

– For $t > 0$, molecules start to diffuse into the nanochannel from both ends until the concentration equilibrates to $c(x, t) = c_b$ at time $t \rightarrow \infty$.

The total number of molecules present in the channel was determined by integrating the numerical solution $c(x, t)$ along the channel length for all time steps t :

$$N(t) = \int_0^L c(x, t) dx$$

This numerical solution $N(t)$ was phenomenologically fitted to the analytical expression

$$N(t) = c_b L \operatorname{erf}\left(2.97 \left(\frac{Dt}{L^2}\right)^{0.6}\right),$$

which does not deviate more than 3% from the numerical solution for all time t (Figure S3).

If molecules are initially present in the nanochannel, i.e. $N(t = 0) \neq c_b L$, the expression for $N(t)$ is modified to

$$N(t) = N(0) + (c_b L - N(0)) \operatorname{erf}\left(2.97 \left(\frac{Dt}{L^2}\right)^{0.6}\right).$$

Since the faradaic current is proportional to the concentration of molecules in the channel, the current $i(t)$ can be expressed as

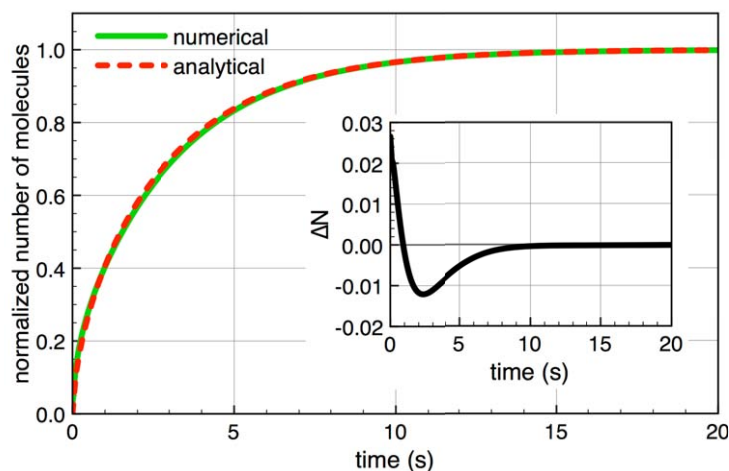


Fig. S4 Comparison of the normalized numerical solution for $N(t)$ (green line) and the analytical expression (dashed red line) for a 10 μm long device with two access holes using $D_{\text{eff}} = 8 \times 10^{-7} \text{ cm}^2/\text{s}$ for both curves. Inset: Difference of the numerical solution and analytical expression.

$$i(t) = i(0) + (i_{ss} - i(0)) \operatorname{erf}\left(2.97 \left(\frac{D t}{L^2}\right)^{0.6}\right),$$

where $i(0)$ is the current at $t = 0$ and i_{ss} is the steady-state current.

For the case of a device with one access hole, molecules can only diffuse into the nanochannel from one end. This corresponds to starting conditions

$$c(x, 0) = 0 \text{ for } x > 0,$$

$$c(x, 0) = c_r \text{ for } x \leq 0,$$

and the boundary conditions

$$c(x=0, t) = c_b,$$

$$\frac{\partial c(x=L, t)}{\partial x} = 0.$$

The numerical solution of the diffusion equation under these conditions is well described by

$$N(t) = c_b L \operatorname{erf}\left(2.97 \times 0.60 \left(\frac{D t}{L^2}\right)^{0.6}\right),$$

and the solution for the diffusion with $N(0)$ molecules present in the channel at $t = 0$ is

$$N(t) = N(0) + (c_b L - N(0)) \operatorname{erf}\left(2.97 \times 0.60 \left(\frac{D t}{L^2}\right)^{0.6}\right).$$

Correspondingly, the current is equal to

$$i(t) = i(0) + (i_{ss} - i(0)) \operatorname{erf}\left(2.97 \times 0.60 \left(\frac{D t}{L^2}\right)^{0.6}\right).$$

D. Multi-potential-step chronoamperometry exhibiting opposite tendencies

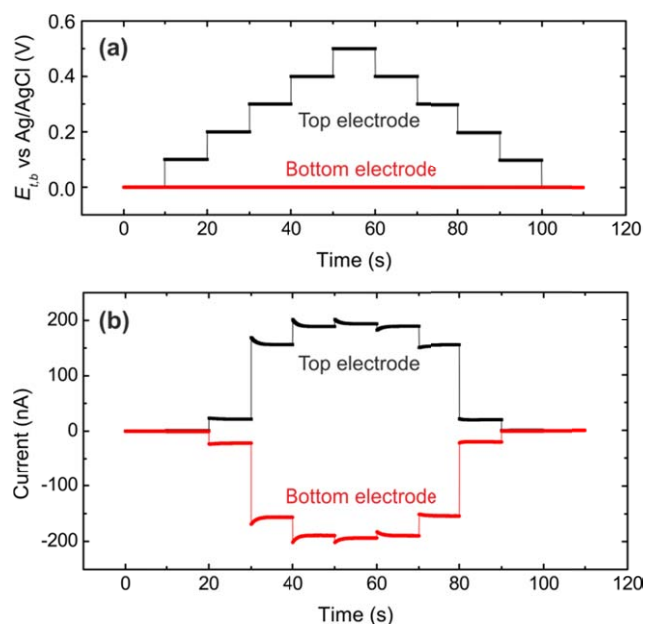


Fig. S5 Multi-potential-step chronoamperometry of a device of type L50H1 filled with an aqueous solution of 1.5 mM $\text{Fc}(\text{MOH})_2$ and 1 M KCl as supporting electrolyte exhibiting tendencies opposite to Figure 2 and 3. (a) Potentials applied as a function of time to the top (black) and bottom (red) electrode. (b) Corresponding current-time response.

Occasionally it was observed that a device whose Cr sacrificial layer was freshly etched exhibited opposite tendencies to those shown in Figure 2 and 3, as shown in Figure S4. When the potential of the oxidizing electrode was stepped up while that of the reducing electrode was maintained at 0 V, the current jumped to a value higher than i_{ss} and gradually returned to the steady-state value; the current fell below i_{ss} when the potential was stepped downwards, then increased again during the transient.